

18

19 **Abstract**

20 High-resolution ocean color observation offers an opportunity to investigate the
21 oceanic small-scale processes. In this study, the Medium Resolution Imaging
22 Spectrometer (MERIS) daily 300-m data were used to study small-scale processes in
23 the western South China Sea. It is indicated that the cyclonic eddies with horizontal
24 scales of 10 km are frequently observed during upwelling season of each year over
25 2004-2009. These small-scale eddies were generated in the vicinity of the southern
26 front of the cold tongue, and then propagated eastward with a speed of approximately
27 12 cm s^{-1} . This propagation speed was consistent with the velocity of the western
28 boundary current. As a result, the small-scale eddies kept rotating high levels of the
29 phytoplankton away from the coastal areas, resulting in the accumulation of
30 phytoplankton in the interior of the eddies. The generation of the small-scale eddies
31 may be associated with strengthening of the relative movement between the rotation
32 speed of the anticyclonic mesoscale eddies and the offshore transport. With the
33 increases of the normalized rotation speed of the anticyclonic mesoscale eddies
34 relative to the offshore transport, the offshore current became meander under the
35 impacts of the anticyclonic mesoscale eddies. The meandered cold tongue and
36 instability front may stimulate the generation of the small-scale eddies. Unidirectional
37 uniform wind along cold tongue may also contribute to the formation of the
38 small-scale eddies.

39

40

42 1. Introduction

43 Approximately 90% of the kinetic energy of ocean circulation is contained in
44 small-scale features, and 50% of the vertical exchange of water mass properties
45 between the upper and the deep ocean may occur at the submesoscale and mesoscale
46 (Bouffard et al., 2012). Mesoscale eddies with horizontal scales of 50-500 km can be
47 observed using altimeters. However, the smaller scale eddies (with horizontal scales
48 below 50 km) cannot be resolved by conventional altimeters (Liu et al., 2008).
49 Satellite ocean color sensors provide high-quality observations of the bio-optical
50 constitute at a spatial resolution better than altimeters. The spatial resolutions of most
51 ocean color satellites fall in the range of 300 m to 1.1 km (at nadir viewing). The
52 high-resolution bio-optical observations reveal more details of small-scale
53 phytoplankton structures. By tracking these small-scale biological features, one can
54 determine the circulation pattern if the motion speed is large with respect of the
55 growth and grazing of the phytoplankton (Pegau et al., 2002). Recently, the Medium
56 Resolution Imaging Spectrometer (MERIS) full-resolution (FR, 300 m) data set is
57 available publicly. The MERIS FR (300 m) phytoplankton fields are rich in smaller
58 scale biological features and provide opportunities to study the small-scale processes.
59 Generally, the time period of the small-scale ocean variability ranges from several
60 days to several weeks. However, the widely used ocean color data are usually
61 averaged into weekly or monthly products in order to obtain a large spatial coverage.
62 This time-averaging may smooth the phytoplankton variability on day-scale (Genin
63 and Boehlert, 1985). Therefore, the study of the small-scale processes requires higher
64 space-time resolution of ocean color observation.

65 The South China Sea (SCS) is the largest marginal basin within the western
66 Pacific, with a total area of 3.5 million km² and a basin depth of > 3000 m (0°–25°N,
67 100°–125°E, figure 1). The SCS is oligotrophic with limited nitrogen and phosphorus
68 within the euphotic layer. A high abundance of phytoplankton mainly occurs in the
69 Gulf of Tonkin, the western South China Sea (SCS) and the Sunda Shelf in summer
70 (Ning et al., 2004). It was reported that a phytoplankton filament in the western SCS
71 is consistent with the mesoscale eddies transportation and Ekman upwelling (Tang et
72 al., 2004; Xie et al., 2003; Xiu and Chai, 2011). However, there have been only
73 limited studies on the small-scale process and its phytoplankton footprints (Nicholson,
74 2012). In this study, the daily MERIS FR data were used to identify the phytoplankton
75 variability associated with the small-scale dynamic processes. In this paper, we will
76 call eddies with diameters smaller than 50 km the small-scale eddies, although in
77 some literatures, they were often called sub-mesoscale eddies (Bassin et al., 2005;
78 Burrage et al., 2009).

79 The western SCS is one of the dynamically active regions in the SCS (Liu et al.,
80 2000). A northeastward alongshore current in summer (figure 1) and a southwestward
81 alongshore current in winter off the east coast of Vietnam are in accordance with wind
82 stress (Hwang and Chen, 2000; Morimoto et al., 2000; Yuan et al., 2005). The
83 northeastward alongshore current meanders off the southeastern coast of Vietnam and

84 leaves the Vietnam coast forming an eastward current driven by the southwest wind
 85 paralleled to the coast of eastern Vietnam (Hwang and Chen, 2000; Kuo et al., 2000;
 86 Barthel et al., 2009). The southwesterly monsoon and Ekman transport drive seasonal
 87 upwelling off southeastern Vietnam coast in summer, leading to more than 1°C drop
 88 in sea surface temperature (SST) (Wyrтки, 1961; Kuo et al., 2000; Metzger, 2003;
 89 Tang et al., 2006). A cold SST tongue around 12°N extends eastward. The orographic
 90 effect of coastal mountain ridge in the Vietnam can further intensify the southwesterly
 91 wind, and thus significantly enhances the coastal upwelling (Xie et al., 2003; Xie et
 92 al., 2007). The local orographic wind forces the coastal jet separation. This
 93 deformation and movement of coastal water induce mesoscale eddy activities (Gan et
 94 al., 2006; Wang et al., 2008; Chen et al., 2010). An eddy pair in the western SCS
 95 during upwelling season are generated probably due to the vorticity transports from
 96 the nonlinear effect of the western boundary currents (Xie et al., 2003; Ning et al.,
 97 2004; Wang et al., 2006; Chen et al., 2010). Moreover, a pair of anticyclonic eddies
 98 (A-A eddies pairs) in the western SCS during the upwelling season was mentioned by
 99 Kuo et al. (2000) and Xie et al. (2003).

100

101 **2. Data**

102 The study area locates in the western SCS, covering from 5°N-18°N,
 103 105°E-115°E (figure 1). The daily MERIS FR chlorophyll data from 2004 to 2009
 104 were obtained from the European Space Agency (ESA). The daily 1 km
 105 Moderate-resolution Imaging Spectroradiometer (MODIS) SST data were obtained
 106 from National Aeronautics and Space Administration (NASA) Ocean Color project.

107 The mean sea level anomaly (MSLA) and geostrophic velocity data used here
 108 were extracted from the Delayed-Time Reference Series provided by Archiving,
 109 Validation and Interpretation of Satellite Data in Oceanography (AVISO). The
 110 mesoscale eddies were identified by a new SSH-based (sea surface height) method
 111 developed by Chelton et al. (2011). Rotational speed was computed by

$$112 \quad U = gf^{-1}A/L_s$$

113 Where g is the gravitational acceleration, f is the Coriolis parameter, A is the
 114 eddy amplitude (in centimetres) and L_s is the eddy length scale (in kilometres),
 115 defined by the radius of the circle that has the same area as the region within the
 116 closed contour of MSLA with maximum average geostrophic current speed (Chelton
 117 *et al.*, 2011).

118 The wind stress was obtained from the National Oceanic and Atmospheric
 119 Administration (NOAA) Environmental Research Division's Data Access Program
 120 (ERDDAP). The offshore transport (M_x) was calculated from

$$121 \quad M_x = \tau_y / f$$

122 Where τ_y is the wind stress parallel to the coastline, positive northward. It was
 123 replaced with the meridional direction wind stress since the most significant offshore

124 transport perpendicular to the Vietnam coast is approximately in the zonal direction.

125 **3. Results and discussion**

126 A series of small cyclonic phytoplankton tendrils at the southern edge of the
127 phytoplankton filament were found during June and October each year over
128 2004-2009 (figure 2). The phytoplankton tendrils had a mean diameter of 25 km and
129 obviously rotated out of the filament as the concentration variability of the
130 phytoplankton tendril seemed consistent with the phytoplankton filament
131 concentration variability. It is implied that the phytoplankton tendril is rotated by the
132 small-scale cyclonic eddy. High levels of phytoplankton were frequently observed in
133 the center of the small-scale cyclonic eddies. The reason for this phenomenon will be
134 discussed in the next section.

135 Figure 3 shows an evolution of two cyclonic phytoplankton tendrils during 9 July
136 2008 and 13 July 2008. It seems that these phytoplankton tendrils have a time scale of
137 several days. The phytoplankton tendril “A” was less obvious on 9 July 2008. Three
138 days later, the concentration of phytoplankton tendril “A” increased about 0.1 mg m^{-3} .
139 This high level of phytoplankton mainly occurred at the edge. The phytoplankton
140 levels in the center were relative low (approximately 0.07 mg m^{-3}). Only one day later,
141 the phytoplankton concentration in the center increased to approximately 0.3 mg m^{-3}
142 and became greater than the level of phytoplankton at the periphery. Another feature
143 was that the cyclonic “A” tended to propagate eastward. It propagated approximately
144 0.1° ($\sim 10 \text{ km}$) from 12 July 2008 to 13 July 2008. The western boundary current had a
145 speed of about 12 cm s^{-1} (10.4 km d^{-1}) in the western SCS during summer (Cai et al.,
146 2007), which was consistent with the propagation velocity of the small cyclonic eddy
147 “A”. Therefore, the eastward propagating cyclonic eddy may be driven by the western
148 boundary current. The small cyclonic eddy B strengthened on 12 July 2008, with high
149 levels of phytoplankton within its interior. And then it disappeared on 13 July 2008.

150 The observation of more detailed phytoplankton distribution in the tendrils was
151 attributed to the much finer resolution (300 m). We found that there were relative high
152 phytoplankton levels in the center of the small cyclonic eddies. One possible
153 mechanism is that the small cyclonic eddies keep rotating high phytoplankton and
154 perhaps nutrients, leading to the accumulation of phytoplankton in their center.
155 Another possible mechanism is that the vertical velocity of these small-scale cyclonic
156 eddies may drive episodic nutrient pulses to the euphotic zone to stimulate
157 phytoplankton growth (Lévy et al., 2012). Figure 4 shows the sea surface temperature
158 distribution associated with the phytoplankton tendril “A”. It is obvious that the cold
159 water was transported away from the cold tongue by the small-scale eddies. And the
160 low temperature water firstly occurred in the periphery of the eddies. Different from
161 the majority of mesoscale cyclonic eddy, there was not significant lower temperature
162 water in the center. It is implied that there is no upwelling or vertical mixing in the
163 center. Therefore, the phytoplankton distribution over this small-scale eddy may be
164 dominated by horizontal movement, and the relative high phytoplankton level in the
165 center of the cyclonic eddies “A” could be attributed to the accumulation of

166 phytoplankton or nutrients from the outer edge to interior under the rotation effect.
167 The small-scale eddies strengthened the horizontal diffusion of the nutrients and
168 phytoplankton (Capet et al., 2008a). These small cyclonic eddies were mainly
169 observed at the front of the filament, where strong differences in water mass
170 properties resulted in high strain rates and instabilities. Meanwhile, the small-scale
171 eddies were also associated with the occurrence of an anticyclonic mesoscale eddy to
172 the south of the filament (figure 3(a)). However, the small-scale cyclonic eddy did not
173 occur for the entire period of the offshore Ekman transport and the anticyclonic eddy.
174 It only arised at certain stages. We analyzed the offshore Ekman transport (M_x) and
175 rotation speed of the anticyclonic eddies during the development of the small-scale
176 eddies over the period of July 2008 shown in figure 3. Due to the limits of the cloud
177 coverage and satellite passing time, the image showing the declination of small-scale
178 eddies was not available. However, it is found that the small-scale eddies disappeared
179 on 22 July 2008. Figure 3 (a) and (b) imply that the small-scale eddies may initially
180 form on 9 July 2008. Therefore, we presumed that the small-scale eddies occurred
181 during the 9-22 July. Figure 5 indicates that the offshore transport (M_x) decreased
182 first and then increased rapidly on 16 July. Different from the variability of M_x , the
183 rotation speed increased from 0.33 m s^{-1} on 2 July to 0.42 m s^{-1} on 12 July. And then it
184 started to decrease to approximately 0.4 m s^{-1} on 16 July. At last, the rotation speed
185 increased associated with the strengthening of M_x . The variability of M_x seemed not
186 consistent with the variability of the levels of phytoplankton (figure 3). The levels of
187 phytoplankton had a significant increases from 9 July to 13 July, accompanying with
188 the decreases of the M_x . This may be due to a lag between nutrients input and
189 phytoplankton growth. The normalized rotation speed of the anticyclonic eddy was
190 defined as the ratio of the rotation speed and the M_x , which indicated the relative
191 movement between the anticyclonic eddy and the offshore transport. The variability
192 of the normalized rotation speed shows that the small-scale eddies was associated
193 with the greater relative movement between the anticyclonic eddy and the offshore
194 transport (figure 5). The offshore current became meander under the influence of the
195 anticyclonic eddy when the offshore transport turned weaker and the rotation speed of
196 the anticyclonic eddy increased. The meandering current may stimulate the generation
197 of the small-scale process (Capet et al., 2008a, b).

198 The phytoplankton filament was consistent with the cold tongue induced by the
199 offshore Ekman transport, which was associated with negative sea surface height
200 anomaly relative to surround light and warm water. The small-scale eddies extended
201 from the cold tongue along the front. Therefore the heavy and cold water firstly
202 occurred in the periphery of small-scale eddies. Along the front, the transport from the
203 surface heavy water to the light water may be forced by the wind. Throughout the
204 development of the small-scale eddies, the wind direction exhibited some variations
205 (figure 6). Wind blowing varied from west-southwest (WSW) on 2 July 2008 (before
206 the generation of the small-scale eddies) to southwest (SW) on 9-13 July 2008 (during
207 the presence of the small-scale eddies). It implies that the small-scale eddies tend to
208 be associated with the more unidirectional uniform wind blowing along the
209 phytoplankton filament. Under spatially uniform wind forcing, the changed

210 meandering current may be more likely to generate the small-scale structure
211 (McGillicuddy et al., 2007; Mahadevan et al., 2008).

212 **4. Conclusion**

213 This paper describes the small-scale cyclonic eddies in the western SCS. Driven
214 by the small-scale cyclonic eddies, a series of phytoplankton tendrils occur at the
215 southern front of the wind-driven offshore current. These small-scale eddies have
216 horizontal scales less than 50 km and propagate eastward at the speed of 12 cm s^{-1} ,
217 accompanying with offshore current. Offshore current, the mesoscale anticyclonic
218 eddies and wind field may contribute to the generation of the small-scale cyclonic
219 eddies. Horizontal transport by the small-scale cyclonic eddies stimulates the
220 diffusion of the nutrients and phytoplankton of the western SCS.

221 **Acknowledgements**

222 We gratefully thank Ruixin Huang and Ian Jones for helpful comments and
223 suggestions. The MERIS 300 m chlorophyll data was provided by ESA-MOST
224 Dragon 3 Cooperation Programme from the European Space Agency. The sea surface
225 height and geostrophic current data were obtained from the Archiving Validation and
226 Interpretation of Satellite Data in Oceanography (AVISO). The MODIS sea surface
227 temperature was obtained from the NASA ocean color project. The wind stress was
228 obtained from the National Oceanic and Atmospheric Administration (NOAA)
229 Environmental Research Division's Data Access Program (ERDDAP). The research
230 was supported by the "Strategic Priority Research Program" of the Chinese Academy
231 of Sciences (No. XDA11010302), the Public science and technology research funds
232 projects of ocean (No. 201205040-6), the Innovation Group Program of State Key
233 Laboratory of Tropical Oceanography, South China Sea Institute of Oceanology,
234 Chinese Academy of Sciences (No. LTOZZ1201) and the National Natural Science
235 Foundation of China (No. 41006111).

236 **References**

- 237 Barthel, K., Rosland, R., and Thai, N.C.: Modelling the circulation on the continental
238 shelf of the province Khanh Hoa in Vietnam, *J. Marine Syst.*, 77(1-2), 89-113, 2009.
- 239 Bassion, C.J., Washburn, L., Brzezinski, M., and McPhee-Shaw, E.: Sub-mesoscale
240 coastal eddies observed by high frequency radar: A new mechanism for delivering
241 nutrients to kelp forests in the Southern California Bight, *Geophys. Res. Lett.*, 32,
242 L12604, 2005.
- 243 Bouffard, J., Renault, L., Ruiz, S., Pascual, A., Dufau, C., and Tintoré, J.: Sub-surface
244 small-scale eddy dynamics from multi-sensor observations and modeling, *Progr.*
245 *Oceanogr.*, 106, 62-79, 2012.
- 246 Burrage, D.M., Book, J.W., Martin, P.J.: Eddies and filaments of the Western Adriatic
247 Current near Cape Gargano: Analysis and prediction, *J. Marine Syst.*, 78, S205-S226,
248 2009.
- 249 Cai, S., Long, X., and Wang, S.: A model study of the summer Southeast Vietnam
250 Offshore Current in the southern South China Sea, *Cont. Shelf Res.*, 27, 2357-2372,

251 2007.

252 Capet, X., McWilliams, J.C., Molemaker, M.J., and Shchepetkin, A.F.: Mesoscale to
253 submesoscale transition in the California Current System. Part I: Flow structure, eddy
254 flux, and observational tests, *J. Phys. Oceanogr.*, 38, 29–43, 2008a.

255 Capet, X., McWilliams, J.C., Molemaker, M.J., and Shchepetkin, A.F.: Mesoscale to
256 submesoscale transition in the California Current System, Part II: Frontal processes. *J.*
257 *Phys. Oceanogr.*, 38, 44–64, 2008b.

258 Chelton, D.B., Schlax, M.G., and Samelson, R.M.: Global observations of nonlinear
259 mesoscale eddies, *Prog. Oceanogr.*, 91(2), 167-216, 2011.

260 Chen, G., Hou, Y., Zhang, Q., and Chu, X.: The eddy pair off eastern Vietnam:
261 Interannual variability and impact on thermohaline structure, *Cont. Shelf Res.*, 30(7),
262 715-723, 2010.

263 Gan, J., Li, H., Curchitser, E.N., and Haidvogel, D.B.: Modeling South China Sea
264 circulation: Response to seasonal forcing regimes, *J. Geophys. Res.*, 111(C6), C06034,
265 2006.

266 Genin, A., and Boehlert, G.W.: Dynamics of temperature and chlorophyll structures
267 above a seamount: An oceanic experiment, *J. Marine Syst.*, 43(4), 907-924, 1985.

268 Huang, B., Hu, J., Xu, H., Cao, Z., and Wang D.: Phytoplankton community at warm
269 eddies in the northern South China Sea in winter 2003/2004, *Deep-Sea Res. Pt. II*, 57,
270 1792-1798, 2010.

271 Hwang, C., and Chen S.-A.: Circulations and eddies over the South China Sea derived
272 from TOPEX/Poseidon altimetry, *J. Geophys. Res.*, 105(C10), 23943-23965, 2000.

273 Kuo, N.-J., Zheng, Q., and Ho, C.-R.: Satellite Observation of Upwelling along the
274 Western Coast of the South China Sea, *Remote Sens. Environ.*, 74(3), 463-470, 2000.

275 Lévy, M., Ferrari, R., Franks, P.J.S., Martin, A.P., and Rivière, P.: Bringing physics
276 to life at the submesoscale, *Geophys. Res. Lett.*, 39, L14602, 2012.

277 Liu, Y., Weisberg, R.H., and Yuan, Y.: Patterns of upper layer circulation variability
278 in the South China Sea from satellite altimetry using the Self-Organizing Map, *Acta*
279 *Oceanol. Sin.*, 27(Supp.), 129-144, 2008.

280 Liu, Y., Yuan, Y., Su, J., and Jiang, J.: Circulation in the South China Sea in summer
281 of 1998, *Chinese Sci. Bull.*, 45(18), 1648-1655, 2000.

282 Mahadevan, A., Thomas, L.N., and Tandon, A.: Comment on "eddy/wind interactions
283 stimulate extraordinary mid-ocean plankton blooms", *Science*, 320, 448, 2008.

284 McGillicuddy, D.J., Anderson, L.A., Bates, N.R., Bibby, T., Buesseler, K.O., Carlson,
285 C.A., Davis, C.S., Ewart, C., Falkowski, P.G., Goldthwait, S.A., Hansell, D.A.,
286 Jenkins, W.J., Johnson, R., Kosnyrev, V.K., Ledwell, J.R., Li, Q.P., Siegel, D.A., and
287 Steinberg, D.K.: Eddy/wind interactions stimulate extraordinary mid-ocean plankton
288 blooms, *Science*, 316, 1021-1026, 2007.

289 Metzger, E.: Upper Ocean Sensitivity to Wind Forcing in the South China Sea, *J.*
290 *Oceanogr.*, 59(6), 783-798, 2003.

291 Morimoto, A., Yoshimoto, K., and Yanagi, T.: Characteristics of sea surface
292 circulation and eddy field in the South China Sea revealed by satellite altimetric data,
293 *J. Oceanogr.*, 3, 331-344, 2000.

294 Nicholson, S.: Linking small-scale circulation dynamics with large-scale seasonal

295 production (phytoplankton) in the Southern Ocean, 4th CSIR Biennial Conference:
296 Real problems relevant solutions, CSIR, Pretoria, 9-10 October 2012
297 Ning, X., Chai, F., Xue, H., Cai, Y., Liu, C., and Shi, J.: Physical-biological
298 oceanographic coupling influencing phytoplankton and primary production in the
299 South China Sea, *J. Geophys. Res.*, 109(C10), C10005, 2004.
300 Pegau, W., Boss, E., and Martínez, A.: Ocean color observations of eddies during the
301 summer in the Gulf of California, *Geophys. Res. Lett.*, 29(9), 1-3, 2002.
302 Tang, D.L., Kawamura, H., Shi, P., Takahashi, W., Guan, L., Shimada, T., Sakaida, F.,
303 and Isoguchi, O.: Seasonal phytoplankton blooms associated with monsoonal
304 influences and coastal environments in the sea areas either side of the Indochina
305 Peninsula, *J. Geophys. Res.*, 111(G1), G01010, 2006.
306 Tang, D., Kawamura, H., Dien, T., and Lee, M.: Offshore phytoplankton biomass
307 increase and its oceanographic causes in the South China Sea, *Mar. Ecol. Prog. Ser.*
308 268, 31-41, 2004.
309 Wang, G., Chen, D., and Su, J.: Generation and life cycle of the dipole in the South
310 China Sea summer circulation, *J. Geophys. Res.*, 111(C6), C06002, 2006.
311 Wang, G., Chen, D., and Su, J.: Winter Eddy Genesis in the Eastern South China Sea
312 due to Orographic Wind Jets, *J. Phy. Oceanogr.*, 38(3), 726-732, 2008.
313 Wyrтки, K.: *Physical Oceanography of the Southeast Asian waters*, NAGA Rep. 2,
314 195 pp., Scripps Inst. Oceanogr, La Jolla, Calif, 1961.
315 Xie, S.-P., Xie, Q., Wang, D., and Liu, W.T.: Summer upwelling in the South China
316 Sea and its role in regional climate variations, *J. Geophys. Res.*, 108(C8), 3261, 2003.
317 Xie, S.-P., Chang, C.-H., Xie, Q., and Wang D.: Intraseasonal variability in the
318 summer South China Sea: Wind jet, cold filament, and recirculations, *J. Geophys.*
319 *Res.*, 112(C10), C10008, 2007.
320 Xiu, P., and Chai, F.: Modeled biogeochemical responses to mesoscale eddies in the
321 South China Sea, *J. Geophys. Res.*, 116(C10), C10006, 2011.
322 Yuan, Y., Liu, Y., Liao, G., Lou, R., Su, J., and Wang, K.: Calculation of circulation in
323 the South China Sea during summer of 2000 by the modified inverse method, *Acta*
324 *Oceanol. Sin.*, 24(1), 14-30, 2005.

325 Figure captions

326 Figure 1. (a) Bathymetry of the South China Sea (Unit: m), the red rectangle
327 represents the study area. (b) Mean surface geostrophic currents in June-October of
328 2002-2008.

329

330 Figure 2. Daily 300 m MERIS chlorophyll (unit: mg m^{-3}) on (a)-(b) 5 September 2004,
331 (c)-(d) 22 June 2005, (e)-(f) 7 June 2006, (g)-(h) 21 July 2007, (i)-(j) 16 July 2008,
332 (k)-(l) 29 July 2009. The cloud covered area was masked by the white color.

333

334 Figure 3. Daily 300 m MERIS chlorophyll (unit: mg m^{-3}) on (a) 9 July 2008, (b) 12
335 July 2008, (c) 13 July 2008. The cloud covered area was masked by the white color.
336 'A' and 'B' indicate two small cyclonic eddies respectively. The pink circle in (a)
337 denotes the anticyclonic mesoscale eddy (AME) on 9 July 2008, which was derived
338 from AVISO MSLA data following the method of Chelton et al. (2011).

339

340 Figure 4. MODIS 1 km sea surface temperature distribution (unit: $^{\circ}\text{C}$) on 13 July
341 2008.

342

343

344 Figure 5. The offshore transport (M_x , $\text{kg m}^{-1} \text{s}^{-1}$), rotation speed of the mesoscale
345 anticyclonic eddy (U , cm s^{-1}) and the normalized rotation speed to M_x (U/M_x),
346 indicating the relative importance of the mesoscale anticyclonic eddy and offshore
347 Ekman transport in the form of small-scale eddies.

348

349 Figure 6. Wind field on 2 July 2008 (the blue arrow), 12 July 2008 (the red arrow)
350 and 26 July 2008 (the green arrow).

351

352

353

354

355

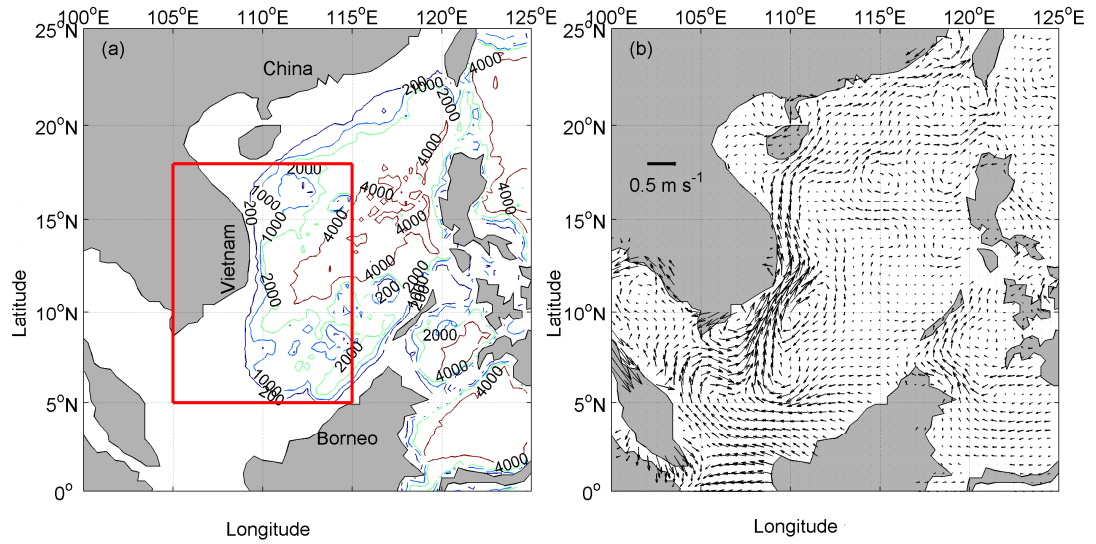
356

357

358

359 Figures

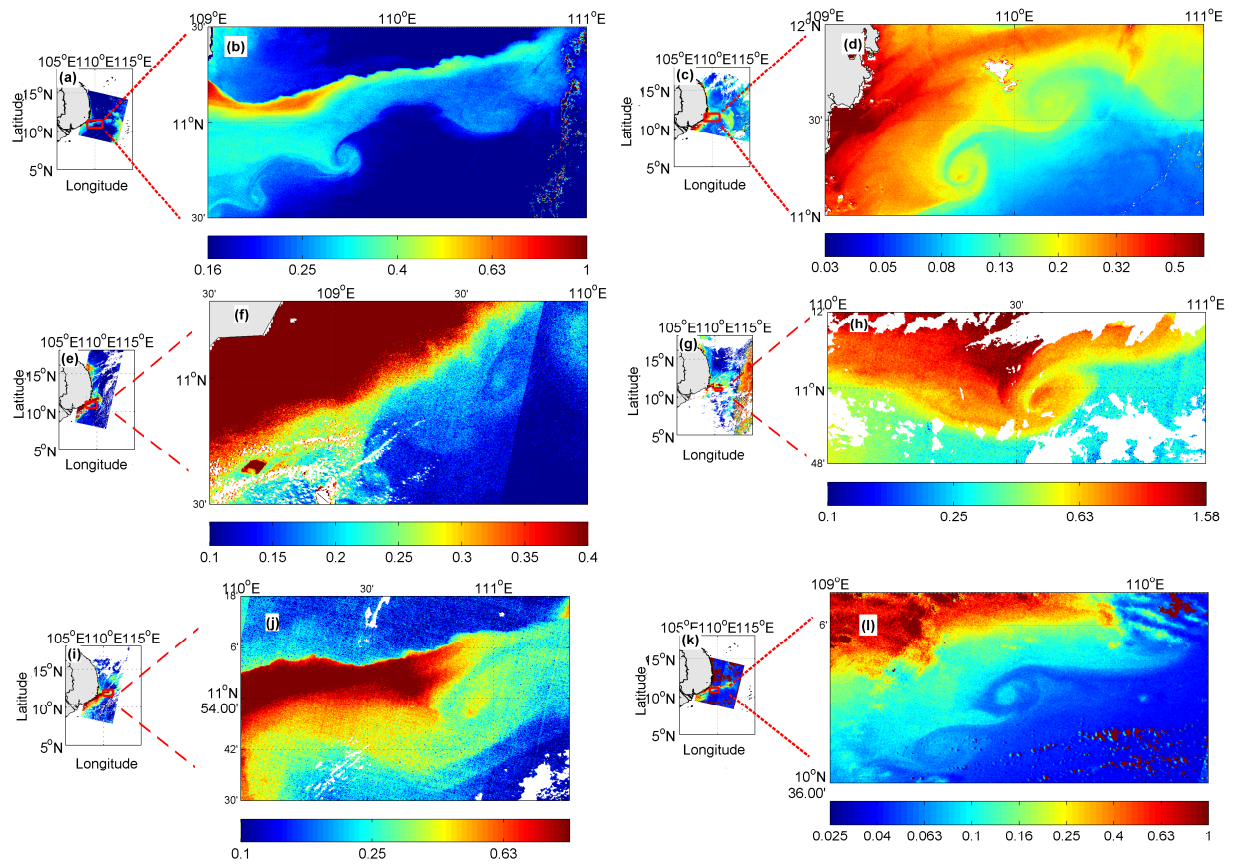
360 Figure 1



361

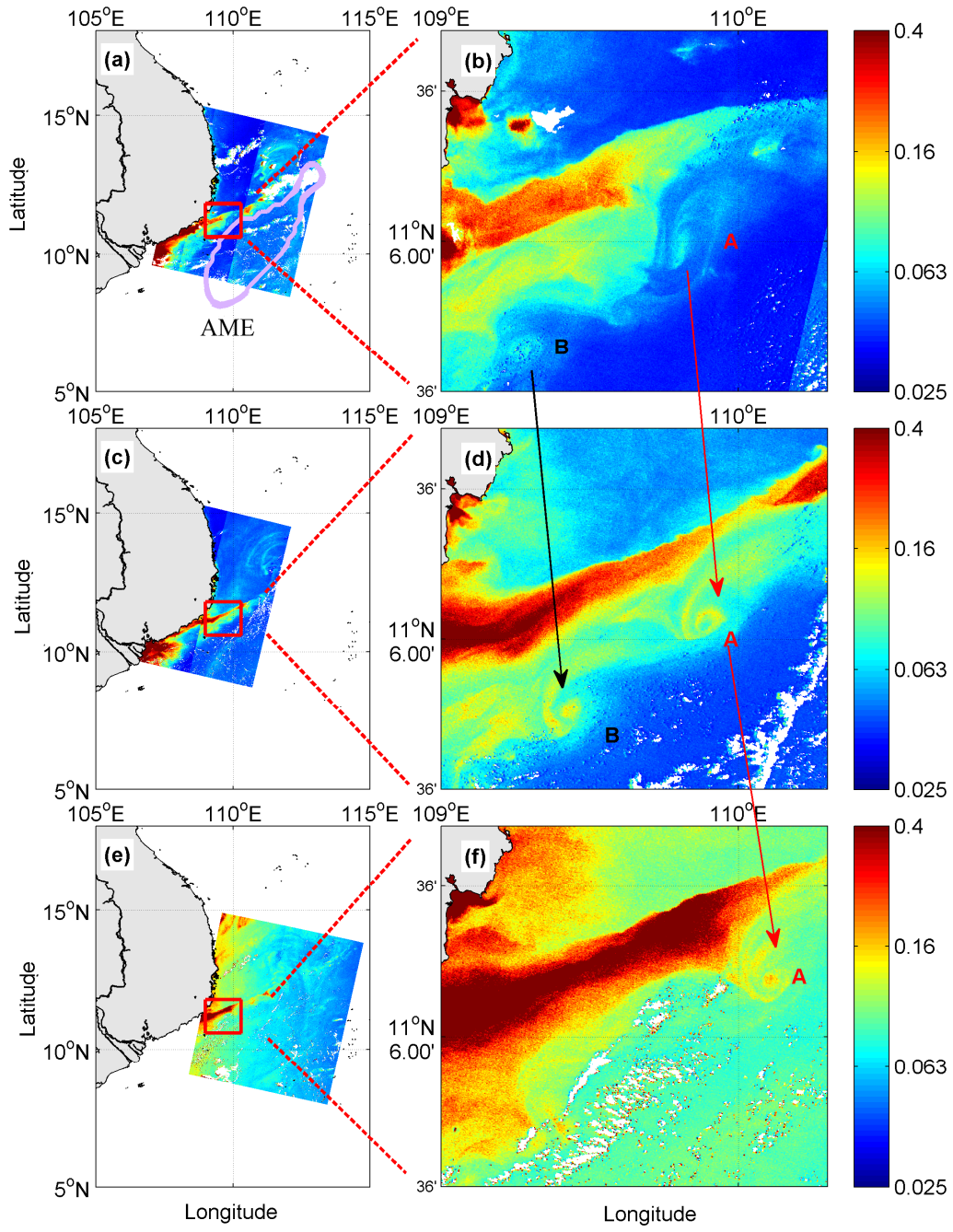
362

363 Figure 2



364

365 Figure 3



366

367

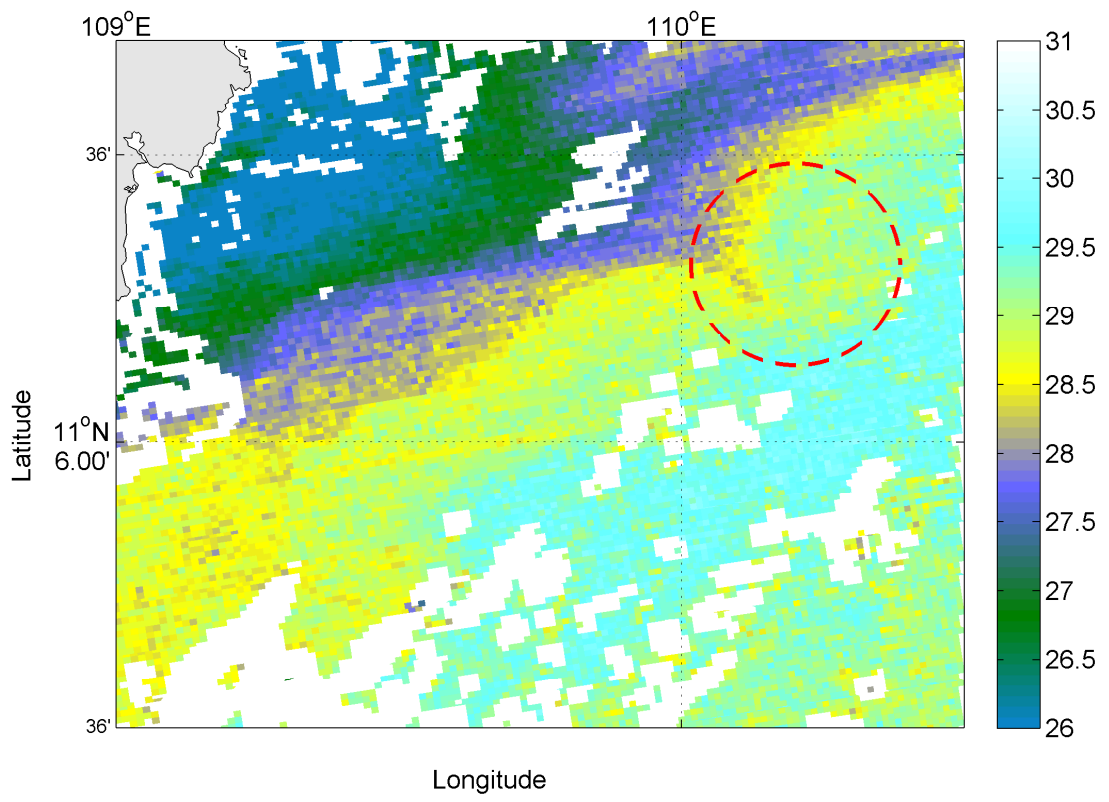
368

369

370

371

372 Figure 4



373

374

375

376

377

378

379

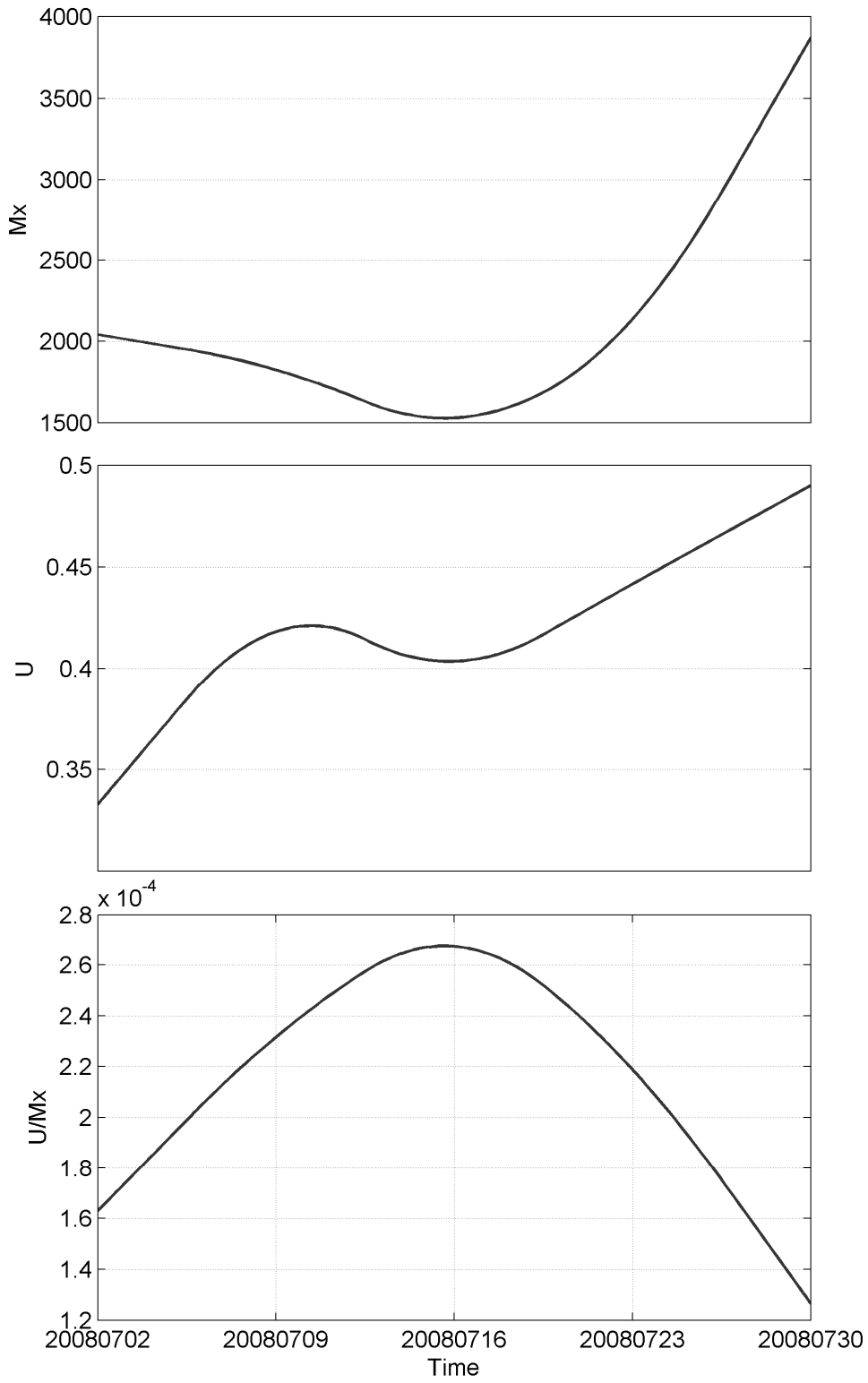
380

381

382

383

384 Figure 5

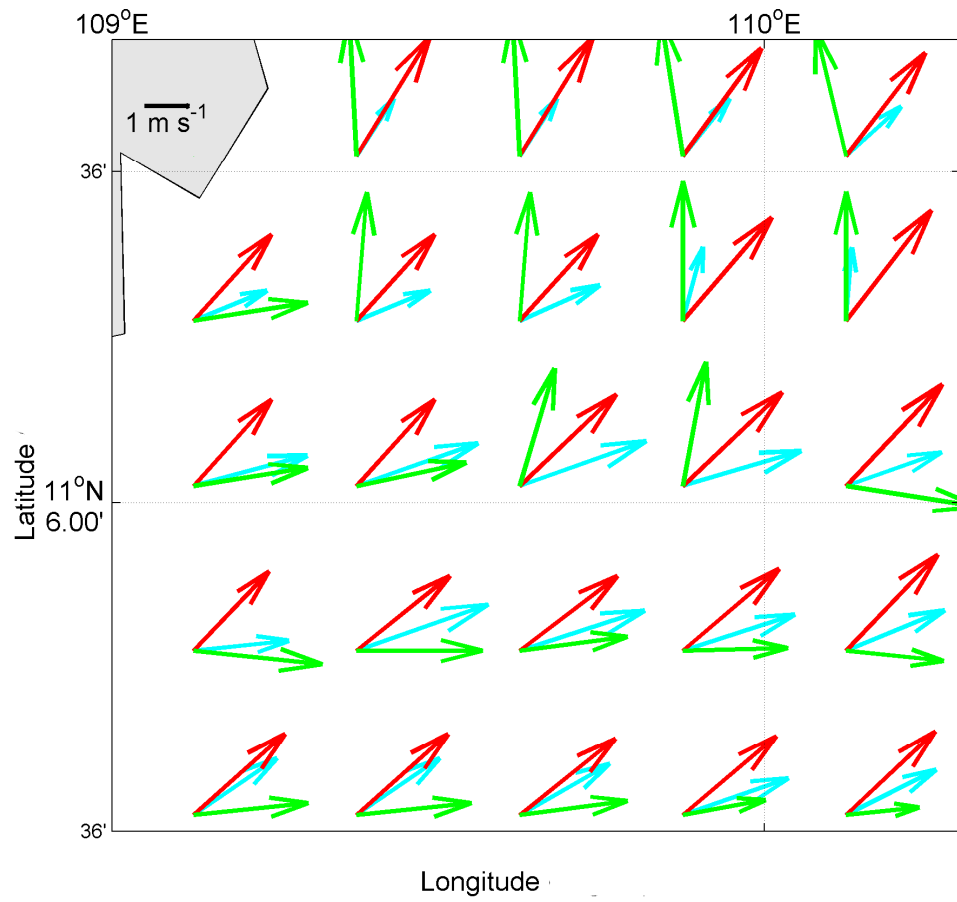


385

386

387

388 Figure 6



389

390

391